Author(s): White, Jai; Terekhina, Irina; Campos dos Santos, Egon; Martín-Yerga, Daniel; Pettersson, Lars G. M.; Johnsson, Mats; Cornell, Ann

Title: Synergistic Bimetallic PdNi Nanoparticles : Enhancing Glycerol Electrooxidation While Preserving C3 Product Selectivity

Year: 2024

Version: Published version

Please cite the original version:

White, J., Terekhina, I., Campos dos Santos, E., Martín-Yerga, D., Pettersson, L. G. M., Johnsson, M., & Cornell, A. (2024). Synergistic Bimetallic PdNi Nanoparticles : Enhancing Glycerol Electrooxidation While Preserving C3 Product Selectivity. ACS Applied Energy Materials, 7(5), 1802-1813. https://doi.org/10.1021/acsaem.3c02789

ACS APPLIED ENERGY MATERIALS

www.acsaem.org
Article

Synergistic Bimetallic PdNi Nanoparticles: Enhancing Glycerol Electrooxidation While Preserving C3 Product Selectivity

Jai White,* Irina Terekhina, Egon Campos dos Santos,* Daniel Martín-Yerga, Lars G. M. Pettersson, Mats Johnsson, and Ann Cornell

Cite This: *ACS Appl. Energy Mater.* 2024, 7, 1802−1813
Read Online

ABSTRACT: Electrochemical conversion of glycerol offers a promising route to synthesize value-added glycerol oxidation products (GOPs) from an abundant biomass-based resource. While noble metals provide a low overpotential for the glycerol electrooxidation reaction (GEOR) and high selectivity toward three-carbon (C3) GOPs, their efficiency and cost can be improved by incorporating non-noble metals. Here, we introduce an effective strategy to enhance the performance of Pd nanoparticles for the GEOR by alloying them with Ni. The resulting PdNi nanoparticles show a significant increase in both specific activity (by almost 60%) and mass activity (by almost 35%) during the GEOR at 40 °C. Additionally, they exhibit higher resistance to deactivation compared to pure Pd. Analysis of the GOPs reveals that the addition of Ni into Pd does not compromise the selectivity, with glycerate remaining at around 60% of the product fraction and the other major product being lactate at around 30%. Density functional theory calculations confirm the reaction pathways and the basis for the higher activity of PdNi. This study demonstrates a significant increase in the GEOR catalytic performance while maintaining the selectivity for C3 GOPs, using a more cost-effective nanocatalyst.

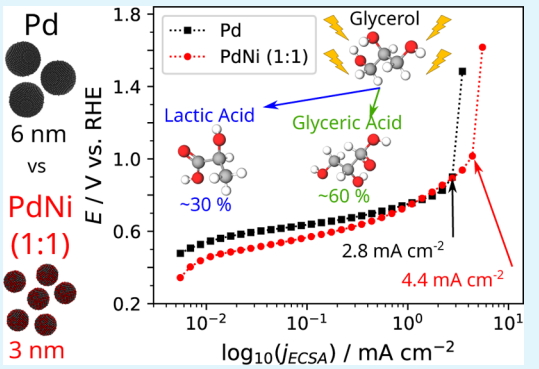

KEYWORDS: *alkaline, electrocatalysis, density functional theory, HPLC, value-added products*

INTRODUCTION

In recent years, biodiesel has emerged as a promising biofuel derived from vegetable oils, animal fat, and their residues.[1,2] The production of biodiesel generates glycerol (Gly) as a significant byproduct, accounting for approximately 10 wt % of the biodiesel produced.[3] The global growth of the biodiesel industry has resulted in a surplus of Gly, causing its market price to decline.[4,5] Consequently, there is growing interest in converting this excess Gly into commercially valuable chemicals. One promising approach for Gly valorization is through the Gly electrooxidation reaction (GEOR), which enables the simultaneous production of valuable chemicals on the anode from Gly and hydrogen on the cathode with lower energy requirements than conventional water electrolysis.[5]

Non-noble and noble metal-based bimetallic and trimetallic electrocatalysts have shown remarkable results for the GEOR by achieving higher activity than the monometallic counterparts.[6−10] Among these, Pd-based nanocatalysts exhibit great potential for the GEOR due to their outstanding performance in alkaline environments, similar cost and abundance to Pt,[11] and lower susceptibility to CO poisoning.[12] Although in the monometallic form, non-noble transition metals such as Ni require a significantly higher potential than Pd to electrochemically oxidize Gly;[13] the addition of such metals to noble metals can significantly enhance the catalytic activity and stability for the GEOR.[11,14−16] Further approaches to improve the catalytic performance of nanomaterials include tuning their morphology and increasing the surface area by introducing porosity or reducing the particle size.[17] The use of PdNi nanocatalysts extends beyond the GEOR to the electrooxidation of other biomass derivatives and organic molecules such as formic acid,[18,19] ethylene glycol,[20] carbohydrazide,[21] ethanol,[22−25] and methanol.[26−28] Aside from nanocatalysts, electrodeposited PdNi films have also been studied for the electrooxidation of lactic[29] and gluconic acids.[30]

The role of Ni in PdNi catalysts in enhancing the electrooxidation of alcohols has been mainly studied for ethanol[25,31,32] and methanol.[27] For ethanol oxidation, the presence of Ni significantly increased the current density compared to pure Pd when Ni served as the surface layer of sputtered PdNi catalysts, in contrast to when it was placed at the sublayer.[32] These findings were supported by density functional theory (DFT) calculations, which assessed the impact of varying

Received: November 4, 2023
Revised: February 12, 2024
Accepted: February 14, 2024
Published: February 29, 2024

Scheme 1. Schematic Representation of the Pd and PdNi Nanoparticle Synthesis

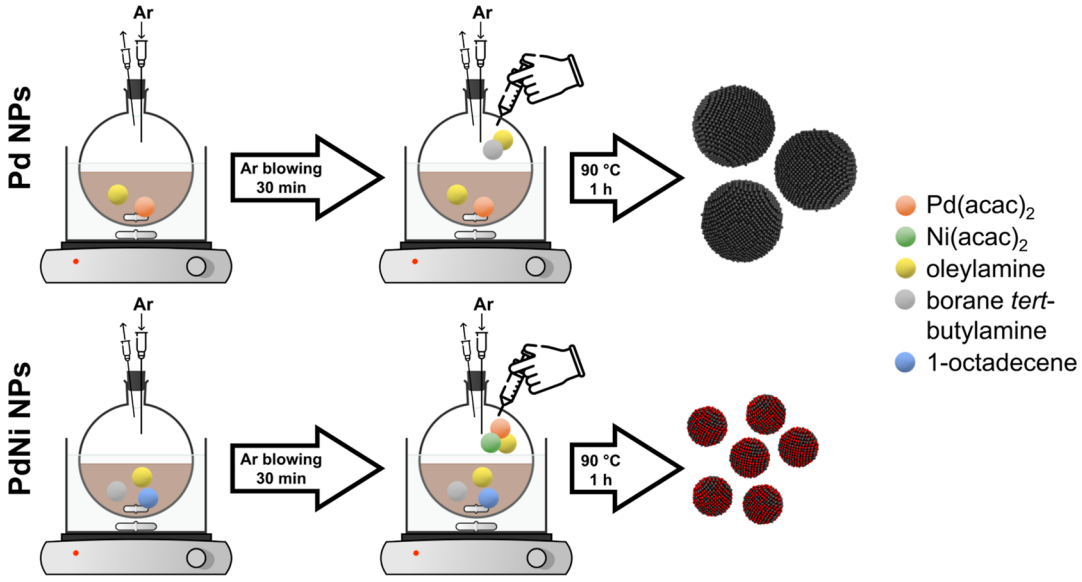

the percentage of surface Ni on a PdNi catalyst with (111) facets.[23] These studies highlight the importance of the structural design of PdNi catalysts. For methanol oxidation, a combined experimental and DFT study revealed that increased Ni concentrations in PdNi nanocatalysts, and specifically $Pd_{0.5}Ni_{0.5}$ (at. %), led to higher selectivity toward CO_2 formation, suppressed CO poisoning, and improved activity for methanol electrooxidation.[27]

For the GEOR, $Pd_{0.5}Ni_{0.5}$ (at. %) nanoparticles (NPs) have shown a higher current density than Pd NPs,[11] which aligns with the general consensus that $Pd_{0.5}Ni_{0.5}$ (at. %) represents the optimal Pd/Ni atomic ratio for Pd-rich catalysts.[14,15] Nevertheless, there is still much to explore regarding the formation of glycerol oxidation products (GOPs) using PdNi electrocatalysts. In alkaline media, Pd-based catalysts typically yield products such as glyceric acid/glycerate (GLA), tartronic acid/tartronate (TTA), oxalic acid/oxalate (OA), glycolic acid/glycolate (GA), and formic acid/formate (FA).[7] However, there are limited reports quantifying GOPs produced by PdNi catalysts.[33] FA, GA, and OA, formed through C−C bond cleavage, are believed to occur at high oxidation potentials,[34] but adsorbed CO has been observed at potentials below the onset of the GEOR on Pd and PdNi nanocatalysts, indicating C−C bond cleavage from a dissociative Gly adsorption step at low potentials.[11] Both scenarios are undesirable because the three carbon (C3) GOPs GLA, LA, and TTA are more valuable due to their uses in important industries such as biomedical (GLA and TTA) and pharmaceuticals (LA),[35] making the mitigation of C−C bond cleavage a primary aim in GEOR developments.

While the typical synthesis of PdNi nanocatalysts involves methods such as coprecipitation, sputtering, electrodeposition, and others, the alloying process can be challenging due to the need for high temperatures, particular additives and reductants, pH adjusters, and multistep synthetic procedures.[36−38] Herein, we report the catalytic performance for the GEOR in alkaline media of sub-10 nm Pd and PdNi NPs, obtained via a modified one-step metal reduction synthesis in organic medium[39] and characterized by transmission electron microscopy (TEM) and powder X-ray diffraction (PXRD). The Pd and PdNi NPs were deposited onto carbon paper electrodes (Pd/C and PdNi/C, respectively), and their electrocatalytic activity was studied by cyclic voltammetry (CV) and *iR*-corrected polarization curves (ICPCs). Galvanostatic electrolysis was employed to generate GOPs, and the product distribution was determined via high-performance liquid chromatography (HPLC), with 90% of the product fractions containing C3 GOPs. DFT calculations confirmed similar reaction pathways for GEOR on Pd(111) and PdNi(111). PdNi/C outperformed Pd/C in terms of both mass and specific activity while exhibiting minimal differences in the distribution of the GOPs. Our study demonstrates the promising performance of PdNi NPs in GEOR by maintaining selectivity for C3 products similar to that of Pd while enhancing the electrocatalytic activity and reducing the overall catalyst cost through a reduction in the required amount of Pd.

EXPERIMENTAL SECTION

Materials and Reagents. Palladium(II) acetylacetonate ($Pd(acac)_2$, Sigma-Aldrich, 99%), nickel(II) acetylacetonate ($Ni(acac)_2$, Combi-Blocks Inc., 98%), oleylamine (OAm, Sigma-Aldrich, technical grade, 70%), borane *tert*-butylamine (BTB, Alfa Aesar, 97%), 1-octadecene (ODA, Sigma-Aldrich, for synthesis), acetone (Honeywell, ≥99.5%), and ethanol (absolute, VWR Chemicals, ≥99.7%) were used for the catalyst synthesis. For the GEOR experiments, the carbon fiber paper (H23, thickness 210 μm, Freudenberg) was cut into 1 cm^2 pieces before hydrophilic treatment. Analytical-grade sodium hydroxide (NaOH, Merck) and Gly (Merck) were both purchased from VWR (Radnor, PA, USA). The ultrapure water (18 MΩ) used to prepare all solutions was obtained with a Millipore DirectQ3 purification system from Millipore (Burlington, MA, USA).

Electrochemical Instrumentation. A Princeton Applied Research PAR273A potentiostat/galvanostat from AMETEK (Minneapolis, MN, USA) was used for electrochemical measurements. To record ICPCs, a current interrupt method was used through the PAR273A in connection with a National Instruments (NI) cDAQ-9178 chassis and a NI9223 voltage digitalizer (Austin, TX, USA), as reported previously.[40] A Hg/HgO reference electrode (RE) (RE-A6P, BioLogic, 1.0 M NaOH) was used for all of the measurements.

Synthesis of Pd and PdNi Electrocatalysts. Pd and PdNi NPs were synthesized via the reduction of $Pd(acac)_2$ and coreduction of $Pd(acac)_2$ and $Ni(acac)_2$, respectively, in an organic medium with OAm serving as a surfactant, BTB as a reducing agent, and ODE as a solvent (see Scheme 1).

Synthesis of Pd Nanoparticles. Pd NPs were synthesized using a modified previously reported procedure.[39] A metal-precursor mixture

https://doi.org/10.1021/acsaem.3c02789
ACS Appl. Energy Mater. 2024, 7, 1802−1813

containing 150 mg of $Pd(acac)_2$ (ca. 0.5 mmol) in 30 mL of OAm in a 50 mL round-bottomed flask equipped with a rubber septum was flushed with argon gas for 30 min to remove excess oxygen. After that, the mixture was heated to 90 °C under magnetic stirring (800 rpm) and an argon atmosphere until it became homogeneous. Next, a reductant-solvent mixture of 600 mg of BTB and 6 mL of OAm, preheated at 60 °C, was quickly injected into the metal-precursor mixture with a syringe. The resulting reaction mixture was allowed to react for 1 h under the same stirring rate and argon stream. The resulting solution was washed by centrifugation four times with an acetone/ethanol mixture (7:3) at 12,000 rpm for 15 min, followed by final redispersion in 1 mL of ethanol and vacuum drying at 60 °C for 24 h.

Synthesis of PdNi Nanoparticles. PdNi NPs were synthesized using a modified previously reported procedure.[39] A reductant-solvent mixture containing 400 mg of BTB, 6 mL of OAm, and 14 mL of ODE in a 50 mL round-bottomed flask equipped with a rubber septum was flushed with argon gas for 30 min to remove excess oxygen. After that, the mixture was heated to 90 °C under magnetic stirring (800 rpm) and an argon atmosphere until it became homogeneous. Next, a metal-precursor mixture of 38.08 mg of $Pd(acac)_2$ (0.125 mmol) and 128.46 mg of $Ni(acac)_2$ (0.300 mmol) in 6 mL of OAm, preheated at 60 °C, was quickly injected into the reductant-solvent mixture with a syringe. The resulting reaction mixture was allowed to react for 1 h under the same stirring rate and argon stream. Finally, the resulting solution was washed, redispersed, and dried similarly to that of the Pd NPs.

The excess Ni precursor introduced in solution is due to the tendency of Pd to be reduced much more readily than Ni. Therefore, to incorporate the desired amount of Ni into the PdNi bimetallic catalyst, a higher Ni content than Pd is required. Since the main goal was to study the performance of PdNi NPs with a Pd/Ni ratio of 1:1, the synthetic procedure was not further optimized to compensate for the losses. The optimization can therefore be a basis for future work and synthetic strategy improvement. Additionally, if the remaining Ni was simply discarded, it would decrease the cost-effectiveness and greenness of the catalyst synthesis process; however, the remaining Ni could easily be recovered as pure Ni through electrodeposition or another reduction process.

Characterization of Electrocatalysts. TEM imaging and energy-dispersive X-ray spectroscopy (EDS) were carried out on a JEOL JEM-2100F microscope operating at an acceleration voltage of 200 kV. TEM samples were prepared by depositing ∼20 μL of NP dispersion in ethanol on a 300-mesh ultrathin Lacey carbon-supported gold grid and allowing the solvent to evaporate. PXRD was performed on a Bruker D8 DISCOVER diffractometer using a Cu Kα X-ray source ($\lambda_{CuK\alpha1}$ = 1.540598 Å and $\lambda_{CuK\alpha2}$ = 1.544426 Å), equipped with an LYNXEYE XE-T detector. The diffractograms were collected within the 2θ range of 10−90° with a step size of 0.01° and scan rate of 0.375°/min.

Electrode Fabrication. The carbon paper working electrode (WE) served as the substrate for drop casting the catalyst ink, following pretreatment by ultrasonication in 3 M HCl, ultrapure water, and ethanol for 15, 10, and 5 min, respectively. It was then dried at 100 °C for 1 h to remove any contaminants and improve hydrophilicity. The catalyst ink was composed of 5 mg of the catalyst (either Pd or PdNi NPs), 5 mg of the Vulcan XC-72 carbon powder, 40 μL of 5% Nafion solution, 240 μL of isopropanol, and 720 μL of ultrapure water, resulting in a catalyst particle concentration of 5 mg mL^{-1}. The catalyst ink was stirred overnight before being drop cast. The drop-casting process involved placing the carbon paper approximately 1.5 cm above a hot plate set at 60 °C. Subsequently, 50 μL of the catalyst ink was drop-cast onto one side of the carbon paper and allowed to dry for 10 min. After drying, the carbon paper was then flipped and an additional 50 μL of the catalyst ink was applied to the other side. After a 10 min drying period, the electrode was removed from the heat and left to dry in air overnight. In total, 0.5 mg of the catalysts were applied to the carbon paper, leading to a Pd mass of 0.5 mg for Pd/C and 0.299 mg of Pd and 0.201 mg of Ni for PdNi/C. The mass of Pd and Ni was determined by eqs S1 and S2, respectively.

Calculations of ECSA. A three-electrode cell (Figure S1) was used to calculate the Pd-based ECSA of Pd/C and PdNi/C by measuring the charge transferred by the reduction of a monolayer of PdO. In this setup, both anodic and cathodic chambers consisted of an N_2-purged 1.0 M NaOH, Gly-free solution at 25 °C with a Nafion (212) membrane dividing the cell. The Nafion membrane was used to mitigate the crossover of GOPs from the anode chamber into the cathode chamber to prevent the possibility of the Pt cathode reducing the formed GOPs. Therefore, the ions passing through the Nafion membrane are most likely Na^+ ions. The catalytic electrode served as the WE, a Pt grid served as the counter electrode (CE) in a 1 M NaOH solution, and the RE was Hg/HgO (1 M NaOH). It has been previously established that a monolayer of PdO is formed in 1 M NaOH at approximately 1.25 V vs RHE,[41] also corroborated in acidic conditions.[42,43] Hence, CV between 0.265 and 1.250 V vs RHE at a sweep rate of 50 mV s^{-1} was initially applied for 20 cycles under solution stirring to stabilize the catalysts.

Then, the solution was held stagnant, and two cyclic voltammograms were recorded within the same potential window and sweep rate. The second cycle was used for ECSA calculation by determining the associated charge of the PdO reduction peak and using eq 1

$$\mathrm{ECSA} = \frac{Q(\mathrm{C})}{S(\mathrm{C/cm^2})} = \frac{\text{area of PdO reduction peak}}{405\ \mu\mathrm{C/cm^2}} \quad (1)$$

where Q is the charge passed during the reduction of PdO to Pd, and S is the characteristic charge density (405 μC cm^{-2}) of the reduction of a monolayer of PdO to Pd.[43]

The ECSA measurements are indicative of the catalysts that were used for the GEOR measurements. Hence, the normalization of the current shown for the Pd and PdNi NPs by the ECSA for the GEOR measurements was done with catalysts that had already been through cycling to the point where the current response was stable.

GEOR Electrochemical Measurements. All GEOR experiments were undertaken in a divided three-electrode cell (Figure S1), with the anode and cathode compartments separated by using a Nafion 212 membrane (VWR). The Pd/C and PdNi/C electrocatalysts were the WEs, a Pt grid was the CE, and the RE was Hg/HgO (1 M NaOH). The WE potential was converted to the reversible hydrogen electrode (RHE) scale using eq 2

$$E_{\mathrm{RHE}} = E^{\mathrm{Ref}}_{\mathrm{Hg/HgO}} + E^{\mathrm{M}}_{\mathrm{Hg/HgO}} + (0.0591 \times \mathrm{pH}) \quad (2)$$

where E_{RHE} is the calculated potential of the electrode in V vs RHE, $E^{Ref}_{Hg/HgO}$ is 0.120 V vs SHE at 25 °C (determined from laboratory measurement), $E^{M}_{Hg/HgO}$ is the measured or controlled potential during the experiments when using Hg/HgO (1 M NaOH), and the pH is 14 as the supporting electrolyte was 1 M NaOH. The respective solutions studied consisted of 0.10 and 0.50 M Gly in 1.0 M NaOH, purged with nitrogen before experiments. The electrochemical measurements were conducted at 25 and 40 °C, with a stirring bar at 200 rpm. The RE was kept at ambient temperature using a Luggin capillary. The activity of the catalysts for GEOR was mainly determined via ICPCs, which were conducted from low to high current densities. Steady-state galvanostatic measurements were used for GOP analysis.

Product Analysis by HPLC. HPLC analyses were performed with an Agilent 1260 Infinity II isocratic pump, multisampler, and multicolumn thermostat with a 1290 Infinity II refractive index detector. The analytical columns, in series, included a Bio-Rad guard column with a standard cartridge holder and a Micro-Guard cation H^+ cartridge (4.6 × 30 mm), Bio-Rad Aminex HPX-87H column (7.8 × 300 mm), and Shodex SUGAR SH1011 column (8 × 300 mm). All columns were kept at 30 °C. To achieve optimal peak separation and ensure accurate results in the analysis of GOPs, two mobile phases were used: 1 mM H_2SO_4 and 8 mM H_2SO_4 at a flow rate of 0.25 mL min^{-1}. The analysis time for each sample was 85 min. All standards for GOPs were calibrated from 0.1 to 10 mM with linear regression R^2 values greater than 0.99. Samples were taken in 100 μL aliquots and diluted with 100 μL of ultrapure water. Chromatograms for each standard analyzed can be seen in Figures S2 and S3.

First-Principles Calculations. The slab models of the catalytic surfaces (Figure S4) were constructed using the atomic simulation environment (ASE).[44] The calculations were carried out on a (4 × 4 ×

https://doi.org/10.1021/acsaem.3c02789
ACS Appl. Energy Mater. 2024, 7, 1802−1813

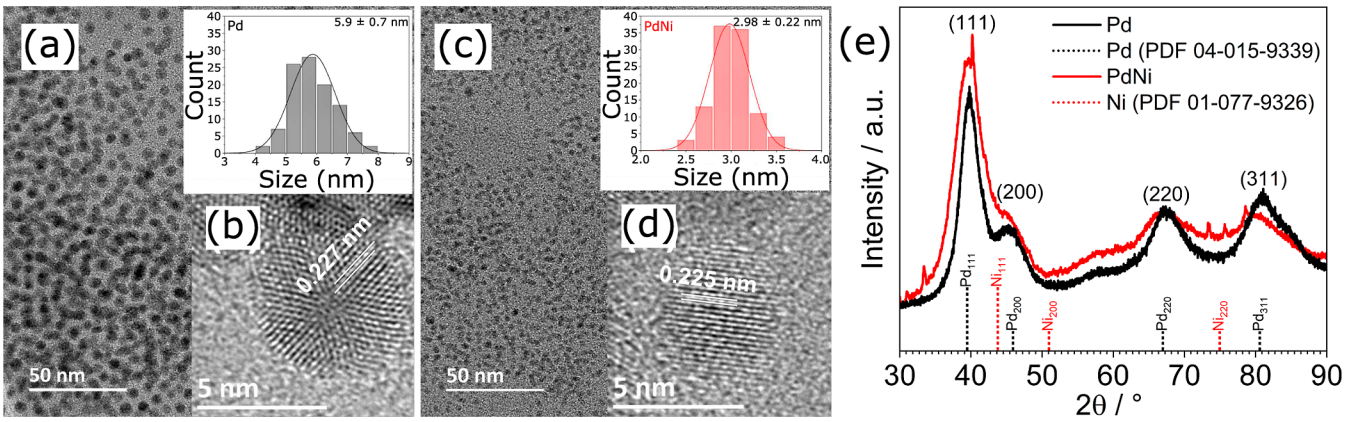

Figure 1. TEM and HRTEM images of (a,b) Pd NPs and (c,d) PdNi NPs. The insets of images (a,b) show particle size distributions of the corresponding catalysts. (e) PXRD patterns of Pd and PdNi NPs.

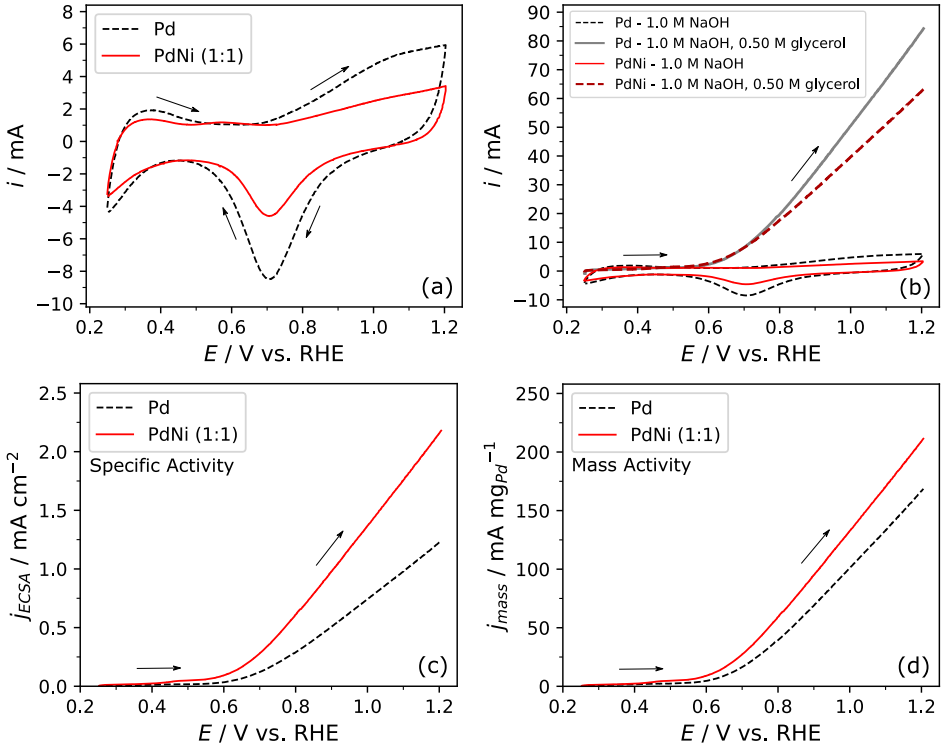

Figure 2. (a) CV in 1.0 M NaOH for Pd/C and PdNi/C. (b) LSV in 1.0 M NaOH and 0.50 M Gly for Pd/C and PdNi/C along with the CV from (a). (c) LSV from (b) normalized by ECSA. (d) LSV from (b) normalized by the mass of Pd in the Pd/C and PdNi/C catalysts. All sweeps were conducted at 25 °C and a sweep rate of 50 mV s^{-1}.

4) slab with a vacuum of 20 Å to avoid interactions between periodic images (Figure S4). The structures were optimized to energy and atom force convergence criteria of 10^{-5} eV and 0.01 eV·Å^{-1}, respectively. Spin-polarized calculations were carried out, and the most stable spin state for all systems is reported in this work. DFT calculations were carried out using the Vienna Ab initio Simulation Package (VASP).[45] The exchange and correlation functional was approximated as the Bayesian error estimation functional, with an additional nonlocal correction term (BEEF-vdW).[46] Potential determining steps (PDSs) were determined following our previous studies.[47,48] As observed in Figures S5−S10, the GEOR was simulated considering three elementary pathways: (1) proton removal, (2) hydrolysis, and (3) hydrogen rearrangement. The DFT total energies were corrected using zero-point energies (ZPEs) and thermal contributions. The harmonic approximation was employed for the vibrational frequency calculations for all of the adsorbates and molecules. Henry's law was used to link the gas-phase pressure to the aqueous concentration using the NIST-JANAF tables.[49] To account for the electrode/electrolyte interface, implicit water solvation was used as implemented in VASP.[50] The electrochemical environment was modeled based on a computational hydrogen electrode.[51] Further information regarding the computational methodology is provided in the Supporting Information.

RESULTS AND DISCUSSION

Characterization of the Nanoparticles. Figure 1a,c shows the TEM images and size distribution histograms of the well-defined Pd and PdNi NPs, respectively. The NPs were monodispersed with a mean particle diameter of 5.9 ± 0.7 nm for Pd and 2.98 ± 0.22 nm for PdNi. The Pd/Ni atomic ratio was nearly 1:1 ($Pd_{0.45}Ni_{0.55}$) as determined by TEM−EDS. HRTEM images of single Pd and PdNi NPs are shown in Figure 1b,d, respectively. The *d*-spacings measured from the lattice fringes, and averaged over 10 individual particles, were 0.227 and 0.225

https://doi.org/10.1021/acsaem.3c02789
ACS Appl. Energy Mater. 2024, 7, 1802−1813

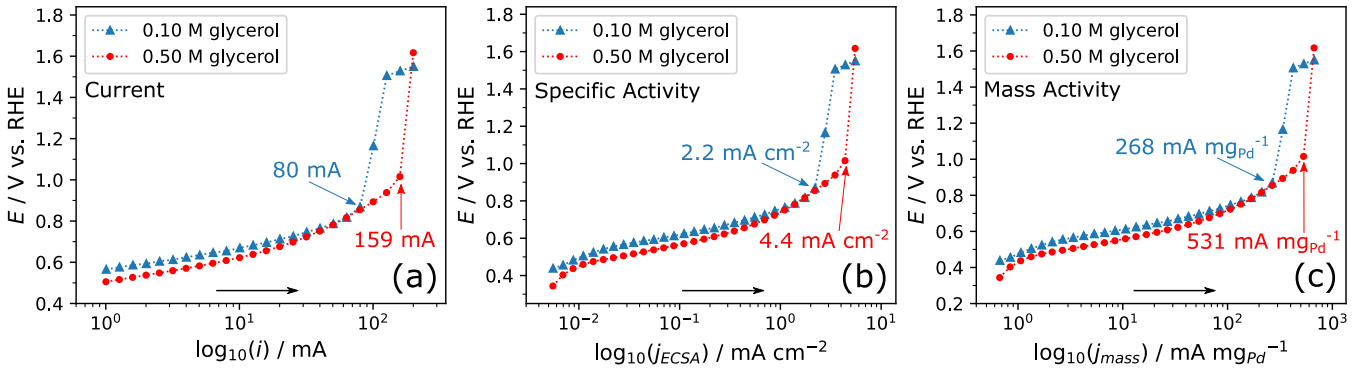

Figure 3. ICPCs for PdNi/C at 40 °C in a supporting electrolyte of 1.0 M NaOH with Gly concentrations of 0.10 M (blue triangles) and 0.50 M (red circles). (a) No normalization, i.e., current; (b) specific activity, i.e., normalized by ECSA; and (c) mass activity, i.e., normalized by the mass of Pd in the PdNi/C catalyst.

nm for Pd and PdNi NPs, respectively, which is close to the lattice spacing for Pd(111) (0.223 nm) and agrees well with d_{111} ≈ 0.22 nm from the corresponding X-ray diffractograms (Figure 1e). The PXRD pattern of Pd NPs shows characteristic diffraction peaks that can be assigned to the (111), (200), (220), and (311) planes, which matched with face-centered cubic Pd (JCPDS 04-015-9339). The PXRD pattern of PdNi NPs exhibits the same features but with peaks widening due to a smaller particle size and a slight shift by ∼0.5° toward the higher 2θ values. The small peaks in the PXRD diffractogram of the PdNi alloy at 74, 76, and 78° are artifacts and not diffraction peaks.

The crystallite sizes were estimated based on the (111) peaks using the Scherrer equation and were found to be 4.71 nm for Pd and 2.46 nm for PdNi NPs, which is slightly smaller than the TEM measurements indicating some polycrystallinity.[39] The characterization demonstrates that the synthesized Pd and PdNi NPs were predominantly composed of Pd(111) and PdNi(111) facets. Additionally, the lattice parameter of PdNi NPs, a_{PdNi} = 3.88 Å, was smaller than that of Pd, a_{Pd} = 3.93 Å, indicating a lattice contraction due to successful alloying by incorporating Ni into the Pd lattice.[52−54]

Electrochemical Characterization. The ECSA of the Pd/C and PdNi/C catalysts was calculated through CV measurements in 1.0 M NaOH (Figure 2a). In the potential window of 0.5 to 1.0 V vs RHE, the cathodic peak is assigned to the reduction of PdO to Pd. The charge associated with this peak for Pd/C led to an ECSA of 68 ± 10 cm^2, slightly more than double that of PdNi/C (29 ± 7 cm^2). The total physical surface area for the PdNi NPs was estimated to be about 2.3 times larger than that of the Pd NPs by considering the mass loading, atomic composition, and morphology, assuming spherical NPs. Given these calculations, the ratio of the available Pd at the surface for Pd NPs to PdNi NPs should be approximately 1:1 using the atomic ratios determined by TEM−EDS. However, the ECSA of PdNi/C is less than half of that of Pd/C. There are two possible reasons that this might be the case.

The first is that the PdNi NPs may have a PdNi alloy composition gradient from the core to the surface with a more Pd-rich core and a more Ni-enriched surface. The second is that the smaller PdNi NPs have a higher packing density due to them being half the size of the Pd NPs, as it has been reported that the smaller the NPs, the higher the packing density.[55] This phenomenon for NPs has been widely reported in the literature.[56−58] However, the PdNi particles in the present study are very small (2.5−3.5 nm), and it is unlikely that there is much segregation in composition when comparing the center and rim of the particles. Additionally, the PXRD pattern for the PdNi alloy in Figure 1e also shows symmetric peaks without shoulders. Therefore, the Pd/Ni ratios determined through TEM−EDS are likely representative of the surface composition, and the decreased ECSA may be a result of the decreased physical surface area due to the packing density of the PdNi NPs. Additionally, based on our previous work on PdNi electrocatalysts for the GEOR,[16,33] the chemical state of Pd and Ni in the PdNi/C catalyst is likely to be elemental Pd and predominantly $Ni(OH)_2$, respectively.

To ascertain the electrochemical response of the GEOR for Pd/C and PdNi/C, linear sweep voltammetry (LSV) was recorded in 1.0 M NaOH and 0.50 M Gly (Figure 2b). The addition of Gly resulted in a significant increase in the anodic current, i.e., the GEOR, with an onset potential of approximately 0.6 V vs RHE for both catalysts. Although the LSV for Pd/C in Figure 2b reaches a higher current (mA) than PdNi/C at the most positive potential, when normalized by the ECSA of the active Pd sites and the mass of Pd in the catalysts, the PdNi/C has higher performance (specific activity: Pd/C = 1.3 mA cm^{-2}; PdNi/C = 2.2 mA cm^{-2}, mass activity: Pd/C = 170 mA mg_{Pd}^{-1}; PdNi/C = 211 mA mg_{Pd}^{-1}). These comparisons can be seen in Figure 2c,d for specific activity and mass activity, respectively. However, given the notable *iR*-drop observed in the LSV, the performance of both electrocatalysts was comparatively evaluated through ICPCs.

To determine the most suitable anolyte for the GEOR, ICPCs for PdNi/C were recorded using two different Gly concentrations, 0.10 and 0.50 M, in a supporting electrolyte of 1.0 M NaOH, see Figure 3. The ICPCs showed a similar trend; as the current is increased, the corresponding potential also increases up until a specific current level is reached, at which point it sharply spikes. This spike represents the deactivation of the catalyst for the GEOR, which occurs due to the oxidation of the active Pd sites.[16,59] The current and corresponding potentials preceding this spike are denoted as the critical current i_{cr} (or critical current density j_{cr}^{ECSA} for specific activity, or critical current when normalized by mass j_{cr}^{mass} for mass activity) and the critical potential E_{cr}, respectively. For 0.50 M Gly solution, the i_{cr}, j_{cr}^{ECSA}, and j_{cr}^{mass} are all approximately double compared to 0.10 M Gly, demonstrating that the higher Gly concentration results in enhanced overall performance for the GEOR. However, despite the fivefold increase in Gly concentration, this did not translate into a fivefold increase in activity. Notably, the PdNi/C catalyst also reached a higher E_{cr} in the solution with a higher Gly

https://doi.org/10.1021/acsaem.3c02789
ACS Appl. Energy Mater. 2024, 7, 1802−1813

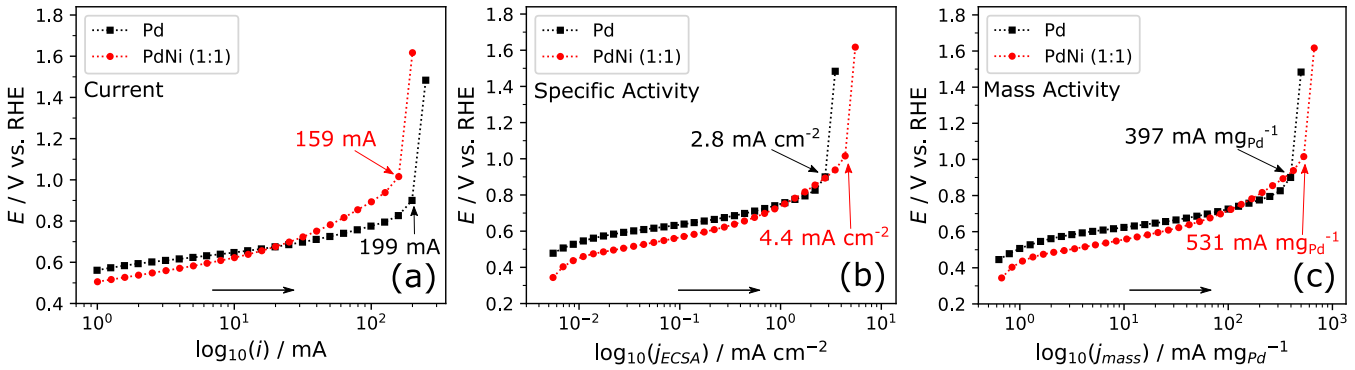

Figure 4. ICPCs for Pd/C (black squares) and PdNi/C (red circles) at 40 °C in a 1.0 M NaOH and 0.50 M Gly solution. (a) No normalization, i.e., current; (b) specific activity, i.e., normalized by ECSA; and (c) mass activity, i.e., normalized by the mass of Pd in the Pd/C and PdNi/C catalysts.

concentration, indicating that catalyst deactivation occurred at a higher potential. Since the 0.50 M Gly solution resulted in i_{cr}, j_{cr}^{ECSA}, j_{cr}^{mass}, and E_{cr} values higher than those of the 0.10 M solution, the former was chosen to compare the performance of Pd/C and PdNi/C at 40 °C.

The comparative ICPCs presented in Figure 4a reveal that the Pd/C catalyst achieves a higher i_{cr} of 199 mA compared to PdNi/C, which exhibits a i_{cr} of 159 mA. This higher i_{cr} is expected since Pd/C has a higher mass of Pd and a larger ECSA than PdNi/C, so the overall current is naturally higher, considering that the GEOR occurs on Pd sites. However, when the data are normalized by ECSA in Figure 4b, PdNi/C emerges as the superior catalyst by active sites for the GEOR. PdNi/C reaches a j_{cr}^{ECSA} of 4.4 mA cm^{-2} compared to that of 2.8 mA cm^{-2} for Pd/C. This represents a 57% increase in specific activity by the PdNi/C catalyst. The significant increase in specific activity for PdNi/C was not equivalently repeated in terms of mass activity. However, the mass activity of PdNi/C shown in Figure 4c reaches a j_{cr}^{mass} of 531 mA mg_{Pd}^{-1} which is 34% higher than that of Pd/C at 397 mA mg_{Pd}^{-1}. Given that the active surface of PdNi/C contains a smaller portion of available Pd than Pd/C, as discussed earlier, these results show that PdNi/C is inherently a more active catalyst for the GEOR, clearly demonstrating the positive role of Ni, at an approximate 1:1 Pd/Ni ratio. Furthermore, since the cost of Pd, at the time of writing, is nearly 2000 times higher than Ni,[60,61] by substituting approximately 40% of Pd, by mass, with Ni in the form of PdNi, a higher j_{cr}^{mass} can be reached at around two-thirds of the cost. Hence, the addition of Ni to Pd NPs enables a superior catalyst at a lower price. In Figure 4a−c, the E_{cr} is consistently higher for PdNi/C than for Pd/C in all three cases, indicating that Pd/C deactivates more readily at a potential lower than that of PdNi/C. This further emphasizes the advantage and superiority of the PdNi/C catalyst.

Since it is well known that for the GEOR, Ni oxidizes Gly at significantly higher potentials than Pd, the Ni present in the PdNi/C catalyst is likely only aiding in the activity of the Pd sites for the GEOR. Indeed, significant work has been done to show that the GEOR on Ni occurs as a result of the oxidation state change in Ni from Ni^{2+} to Ni^{3+} in the forms of $Ni(OH)_2$ and NiOOH, respectively.[62] The oxidation state change occurs around 1.4 V vs RHE, and therefore studies on Ni for the GEOR regularly show the onset potential being around the mentioned voltage. Hence, the GEOR onset potential for Ni compared to Pd is around 700 mV higher.[16] Additionally, an increased onset potential and utilization of monometallic catalysts such as non-noble transition metals like Ni reportedly result in a significant C−C cleavage in highly alkaline conditions and, consequently, decreased yields of highly valued C3 GOPs are reported.[63] This is not the case from the HPLC GOP analysis presented in this study (vide infra).

The reason for the superior performance when noble metals are combined with non-noble metals is a topic of debate in the literature. The two main themes are the bifunctional mechanism and electronic effect. For the bifunctional mechanism, the addition of an oxophilic metal such as Ni to a noble metal catalyst enhances the catalytic activity by providing an increased amount of proximal hydroxide species adjacent to the GEOR active sites.[11,15,64] The enhanced activity is then a result of either the increased hydroxide species providing a more oxidative environment, participating in the GEOR or aiding the oxidative removal of inhibiting CO_{ad} intermediates. For the electronic effect, the addition of non-noble transition metals to the lattice of noble metals such as Pt and Pd decreases the binding energy for inhibiting species such as CO[27] and OH,[65] and it can increase the number of available surface electrons[66] and lower glycerol adsorption energy;[66] the result being easier desorption of intermediates and, therefore, increased active sites during the GEOR as well as less C−C bond cleavage. From the perspective of this study, it is difficult to discern definitively which process explains the increased performance of PdNi/C over Pd/C, but both processes seem plausible. However, the study conducted on PtNi by Luo et al.[65] provides a detailed body of evidence pertaining to the role of Ni in enhancing the catalytic activity of Pt being a result of the electronic effect.

Note that in the present study, we have avoided kinetic analyses from the Tafel slope as calculating Tafel slopes from the ICPCs for the GEOR is problematic, as the reaction mechanism may vary along the polarization curve. Hence, the calculation of such slopes may be misleading and may not give true indications of a single reaction-limiting step.

Glycerol Oxidation Product Analysis. To analyze the GOPs generated by the PdNi/C and Pd/C catalysts, galvanostatic measurements were conducted in 0.50 M Gly in 1.0 M NaOH solutions to a final charge of 18C (Figures S11 and S12). Although long-term stability is an important aspect of electrocatalytic systems, the goal of this study was to synthesize the (111) crystal facet catalysts and directly compare their activity and product distribution experimentally and computationally close to the GEOR onset potential. That is why, for the experimental determination of the GOPs, a small volume of solution was used, and only 18C were passed such that a readable concentration of products could be determined in a short period of time. Further work on these catalysts in a larger

https://doi.org/10.1021/acsaem.3c02789
ACS Appl. Energy Mater. 2024, 7, 1802−1813

Table 1. Product Fractions of GOPs and Glycerol Conversion from Galvanostatic Experiments Using Pd/C and PdNi/C in 0.50 M Gly and 1.0 M NaOH[a]

electrocatalyst, V vs RHE	product fraction average ± standard deviation (%)							Gly conversion (%)
(number of experiments)	GLA	LA	TTA	FA	GA	OA	AA	
PdNi/C, 0.983 ± 0.003 V (1)	56	27	3.8	9.9	0.9	2.3	0	2.4
PdNi/C, 0.846 ± 0.021 V (3)	58 ± 4	29 ± 2	5.3 ± 0.6	1.1 ± 1.2	2.2 ± 1.7	3.6 ± 0.6	0.6 ± 0.4	1.4 ± 0.5
PdNi/C, 0.721 ± 0.015 V (2)	60 ± 1	30 ± 1	6.6 ± 0.1	0.5 ± 0.5	0 ± 0	2.1 ± 0.4	0.6 ± 0.6	1.3 ± 0.6
PdNi/C, 0.688 ± 0.029 V (2)	61 ± 4	30 ± 4	5.5 ± 2.0	1.8 ± 1.8	0 ± 0	1.2 ± 0.5	0.5 ± 0.5	1.6 ± 0.0
Pd/C, 0.832 ± 0.049 V (2)	60 ± 0	24 ± 0	5.9 ± 0.1	5.6 ± 1.0	2.1 ± 2.1	1.8 ± 0.4	1.0 ± 1.0	1.6 ± 0.1
Pd/C, 0.734 ± 0.020 V (3)	62 ± 2	26 ± 2	6.3 ± 0.5	2.0 ± 1.5	1.4 ± 0.6	1.4 ± 0.8	1.6 ± 1.2	1.9 ± 0.2
Pd/C, 0.672 ± 0.022 V (4)	64 ± 2	24 ± 3	8.3 ± 1.3	0.6 ± 0.5	0.5 ± 0.4	2.8 ± 0.9	0.5 ± 0.4	2.3 ± 0.4

[a]18C passed for each measurement.

volume cell setup, in which the catalysts can be used for extended periods to assess the stability, is important to be pursued. However, given that the NPs are somewhat spherical, it would be challenging to detect changes to the morphology or structure of such small particles (6 nm for Pd and 3 nm for PdNi).

The product analysis resulting from the galvanostatic measurements is presented as product fractions of the sum of the overall GOP concentrations in Table 1 and Figure 5 as a function of measured potential. A result of the experiments being performed galvanostatically is that the average potential during the experiments slightly differs between runs. Therefore, the measured potential for each experiment was corrected for the *iR*-drop in the electrochemical cell, and then the average potential, in addition to the standard deviation (SD), was calculated over the entire run. For repeat experiments, the same process was adopted, then a second average and SD were determined for the combined number of experiments. The average and SD of the WE potential are reported in Table 1, which shows that the potentials for the comparison of PdNi/C to Pd/C are not exactly the same but are within the SD. The potentials analyzed were chosen to be close to the GEOR onset because the catalysts become less selective, and C−C bond cleavage is more likely at higher potentials. The GOP concentrations determined by HPLC analysis were normalized by the charge passed and then converted to a fraction.

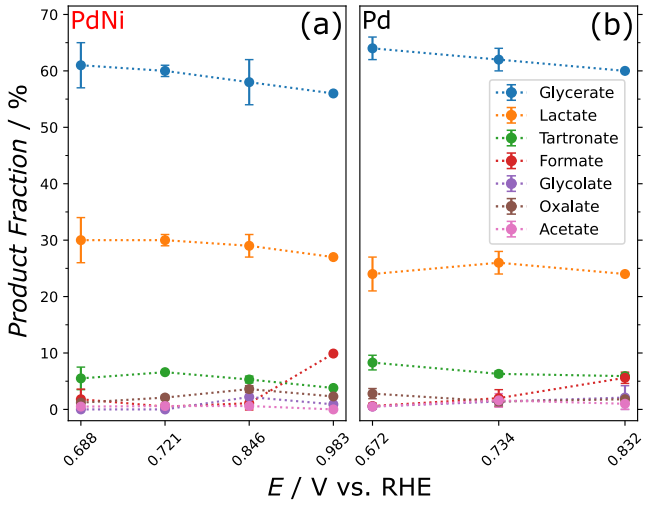

Figure 5. Product fractions analyzed by HPLC for (a) PdNi/C and (b) Pd/C catalysts at varying potentials.

The product fractions listed in Table 1 show that an increased potential for both PdNi/C and Pd/C results in lower product fractions for GLA and LA. Overall, the two main products, GLA and LA, are formed in similar proportions as a function of potential for both PdNi/C and Pd/C. Additionally, to demonstrate C−C cleavage at higher potentials, one experiment was done at 0.983 V vs RHE for PdNi/C leading to a larger product fraction of FA. Figure 5 graphically illustrates the data presented in Table 1 and shows that, remarkably, there is very little difference in the product fraction distribution of the GOPs for Pd/C and PdNi/C with there being a maximum of 3 and 5% differences between the product fractions for GLA and LA, respectively, observed at similar potentials. The Gly conversion % shown in Table 1 is quite low due to the high concentration of Gly in solution and relatively short electrolysis times evaluated, which were done to minimize the chemical reactions that can occur in alkaline solution.

Figure 5 shows a decrease in the selectivity for GLA as the potential increases, for both PdNi/C and Pd/C. At the lowest examined potentials of 0.688 V vs RHE for PdNi/C and 0.672 V vs RHE for Pd/C, the product selectivity to GLA was the highest, with product fractions of 64 and 61%, respectively. This suggests that the closer the anodic potentials are to the GEOR onset potential and likewise to the PDS potential calculated by DFT (vide infra), the higher the selectivity toward the formation of GLA. At higher potentials, comparing PdNi/C and Pd/C at 0.721 V vs RHE and 0.734 V vs RHE, respectively, the GLA product fraction was 60 and 62% for PdNi/C and Pd/C, respectively. Therefore, under the current experimental conditions, the reaction pathway is not significantly altered by the addition of Ni to Pd. Hence, the PdNi/C demonstrates improved electrochemical performance for the GEOR compared to Pd/C, as discussed earlier, without compromising the selectivity for the predominant GLA product.

The second most abundant product was LA. Figure 5 demonstrates that PdNi/C had a slightly higher selectivity to lactate than Pd/C. However, the overall similar product fractions for the two catalysts further illustrate that the reaction pathways are not significantly altered by alloying Ni with Pd. At the highest potential studied for PdNi/C, 0.983 V vs RHE, the product fractions for GLA and LA were the lowest, and there was an increased selectivity to FA compared to lower potentials. This decrease in selectivity for C3 GOPs at higher potentials has also been reported previously.[67,68] The same increase in the FA product fraction at a higher potential also occurred for Pd/C at 0.832 V vs RHE when compared to lower potentials. Interestingly, there was a lower FA product fraction for PdNi/C at 0.846 V vs RHE than for Pd/C at 0.832 V vs RHE, suggesting a lower affinity for C−C bond cleavage.

https://doi.org/10.1021/acsaem.3c02789
ACS Appl. Energy Mater. 2024, 7, 1802−1813

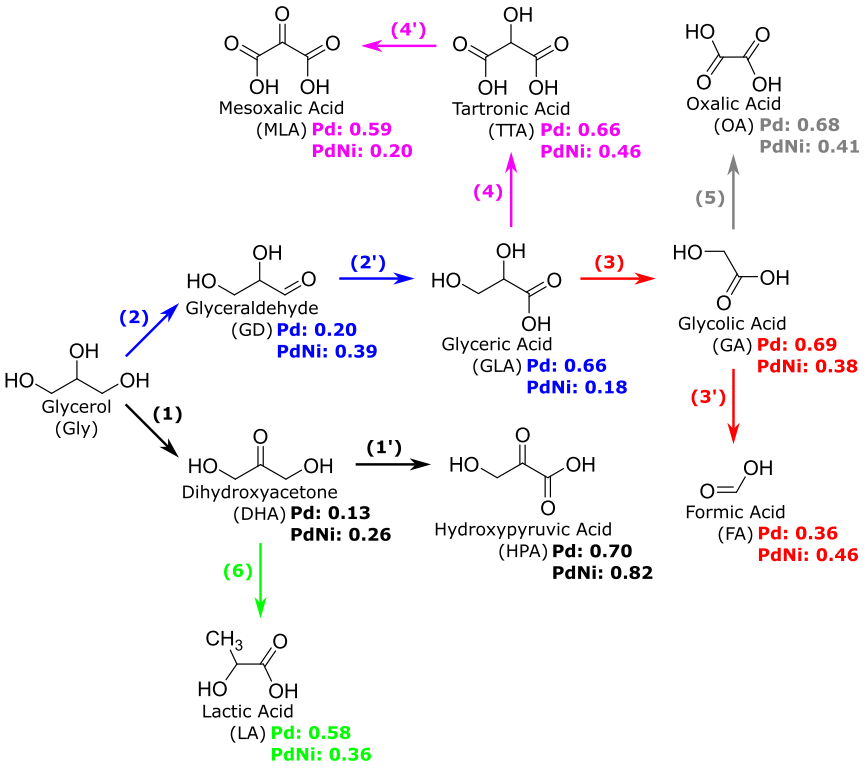

Figure 6. Representation of the calculated Gly electrooxidation pathway of Pd(111) and PdNi(111) catalysts in alkaline solution with PDS values (in eV) of each oxidation step. The oxidation pathway of each intermediate is shown using different colors as follows: (1) Gly−DHA (black), (1′) DHA−HPA (black), (2) Gly−GD (blue), (2′) GD−GLA (blue), (3) GLA−GA (red), (3′) GA−FA (red), (4) GLA−TTA (magenta), (4′) TTA−MLA (magenta), (5) GA−OA (gray), and (6) DHA−LA (green). Here, PDS represents the minimum potential required to overcome the energy barrier of the reactions illustrated in Figures S5−S10.

In comparison to the present study, reports on Pt[69] and PtNi[65,70] in alkaline media have shown varied results as to the main product generated during the GEOR. On a Pt RDE, Melle et al.[69] showed that for supporting electrolytes of LiOH, NaOH, and KOH, LA and GLA are generated in approximately even amounts close to the GEOR onset potential, but for NaOH, LA formation dominates at higher potentials. For PtNi, Luo et al.[65] reported that close to the onset potential for the GEOR (0.5 V vs RHE), Pt/C and $Pt_{1.2}Ni_1$ supported on carbon paper (ratio of Pt/Ni in at. %) had similar selectivity with approximately 40% of the products assigned to GLA and the remaining 60% being TTA. The authors noted that only low quantities of LA were formed. Furthermore, at a higher potential (0.7 V vs RHE), the selectivity toward GLA dropped considerably for both Pt/C and $Pt_{1.2}Ni_1$ to around 20%, whereas in the present study, an increase of around 200 mV from the lowest studied potential shows no such decline in the product fraction of GLA. In contrast to Luo et al.,[65] for Pt and $Pt_{67}Ni_{33}$ supported by graphene nanosheets under an applied potential close to the GEOR onset, Zhou et al.[70] reported GA to be the dominant product in both cases with around 40% selectivity. Additionally, the authors found GD and GLA present in both cases but with Pt having higher selectivity toward GD and $Pt_{67}Ni_{33}$ favoring GLA, whereas in the present study with PdNi, GD was not detected, and GA was a minor product.

In summary, the general trends from the product analysis indicate that PdNi/C maintains the selectivity for GLA and exhibits slightly higher selectivity for LA when compared to Pd/C. The selectivity toward GLA decreases only slightly at higher potentials for both Pd/C and PdNi/C. Despite the increased specific activity for the PdNi/C catalyst compared to Pd/C, it is remarkable that the product selectivity is consistently maintained at various potentials. The similar GEOR pathways for the two catalysts were confirmed through DFT calculations.

Density Functional Theory Calculations. Figure 6 shows the computed PDS for GEOR to form common liquid products. All reactions are labeled from 1 to 6. The oxidation of the secondary hydroxyl group on Gly can undergo either pathway 1, forming dihydroxyacetone (DHA) or hydroxypyruvic acid (HPA) as the major product (Gly−DHA−HPA); or pathway 6, forming DHA or LA as the major product (Gly−DHA−LA). The oxidation of the primary hydroxyl group on Gly follows pathway 2, forming glyceraldehyde (GD) or GLA as the major oxidation product (Gly−GD−GLA).

The Pd and PdNi surfaces require smaller PDS values (Pd: 0.66 eV, PdNi: 0.39 eV) in pathway 1 to form GLA and pathway 6 to form LA (Pd: 0.58 eV, PdNi: 0.36 eV) than following pathway 2 to form HPA (Pd: 0.66 eV, PdNi: 0.39 eV). Table 2 summarizes the PDS required to form the GOPs starting from

Table 2. Calculated PDS Values to Obtain the Liquid Products Are Given in Figure 6[a]

products	reaction	Ci	Pd	PdNi
glycerate	Gly−GD−GLA	C3	0.69	0.39
lactate	Gly−DHA−LA	C3	0.58	0.36
tartronate	Gly−GD−GLA−TTA	C3	0.66	0.46
formate	Gly−GD−GLA−GA−FA	C1	0.69	0.46
glycolate	Gly−GD−GLA−GA	C2	0.69	0.38
oxalate	Gly−GD−GLA−GA−OA	C2	0.68	0.41

[a]All PDS values are in eV.

https://doi.org/10.1021/acsaem.3c02789
ACS Appl. Energy Mater. 2024, 7, 1802−1813

the Gly molecule. The PDSs of GLA and LA are the lowest values, which justifies the higher product fraction of both species obtained by HPLC. For a close-packed Pd structure (Pd(111)), Valter et al.[71,72] found, using DFT calculations, that the first deprotonation step leading to the adsorption of Gly to Pd favors adsorption by the secondary carbon and that after two deprotonation steps, Gly was bound by both primary and secondary carbon. The authors noted that while this form of adsorption should give either GD or DHA, in experimental studies, the GD pathway was more commonly reported with the subsequent oxidation step, in alkaline conditions, forming GLA. Additionally, the authors found that the first adsorption/deprotonation step for Pt(111) mirrored that of Pd(111) but that the second adsorption step likely favored both primary carbons bound to Pt. This may be a reason for the difference in the product distribution observed in the present study compared to that of Pt and PtNi studies in alkaline media discussed earlier.

The experimental product fraction of LA was considerably lower than that of GLA, which can be explained by two main reasons: (i) LA formation involves a series of chemical steps including C−O cleavage (Figure S10), which are not affected by the applied potential and (ii) the interconversion of GD and DHA leads to the LA route as the minor pathway. For (ii), DHA is unstable under alkaline conditions and can be converted into GD or pyruvaldehyde (PV), resulting in either GLA or LA formation, respectively. These conversions are more likely than HPA formation from DHA since the PDS for HPA formation is higher,[73−75] as shown in Figure 6 for reaction (1′). Although the formation of LA from PV is a known reaction,[76] and the DFT calculations show that PV and LA formation from DHA has a common intermediate (Figure S13), the formation of GD from DHA has been shown to have a higher rate constant than PV formation at elevated temperatures in alkaline conditions.[77] Therefore, it is likely that there is a mix of LA, PV, and GD chemically produced after any electrochemical DHA formation but with a preference for the interconversion of DHA to GD. Hence, GLA formation can be achieved electrochemically from GD in greater proportions than the chemical formation of LA mentioned in (i).

Table 2 presents data showing that, for all of the GOPs experimentally detected, PdNi has a lower PDS than Pd. This observation aligns with the experimental findings, indicating that PdNi/C catalysts exhibit superior electrocatalytic activity compared to Pd/C while maintaining selectivity toward valuable GOPs, such as GLA and LA.

CONCLUSIONS

The addition of Ni to Pd to create PdNi NPs has proven to be an effective strategy for improving the performance of the GEOR under alkaline conditions. The novelty of the present study involves the successfully tuned synthesis of pure Pd and alloyed $Pd_{0.45}Ni_{0.55}$ (at. %) NPs, which are very close to the desired pure Pd(111) and PdNi(111) and resulted in nanocatalysts of a certain morphology and composition that were further investigated as promising materials for the GEOR supported by the DFT modeling. Catalyst fabrication procedures usually focus on the composition or morphology; meanwhile, we attempted to fix both aspects. PdNi/C exhibited significantly enhanced specific and mass activity compared to Pd/C, as analyzed by ICPCs. Generally, reports in the literature will show either specific activity or mass activity, but in our study, PdNi was the superior catalyst in both cases. Additionally, PdNi/C was able to operate at potentials higher than those of Pd/C before deactivation by PdO formation. The DFT calculations for the formation of all experimentally detected GOPs consistently indicated lower PDS values for PdNi than Pd, thereby supporting the electrochemical findings. Both PdNi/C and Pd/C displayed high selectivity toward GLA and LA, with product fractions of around 60 and 30%, respectively. At increased potentials, the selectivity for GLA and LA decreased but remained above 50 and 20%, respectively, with PdNi/C exhibiting slightly higher selectivity for LA than Pd/C. This study combines experimental and computational approaches to unambiguously establish that bimetallic PdNi NPs are promising electrocatalysts for the GEOR, significantly improving the activity compared to monometallic Pd while maintaining the selectivity for valuable GOPs. The number of studies including the quantitative analysis of GOPs using HPLC for PdNi catalysts, especially coupled with DFT calculations, is limited in the literature; hence, the findings of the present study provide new insights for the field.

ASSOCIATED CONTENT

Supporting Information

The Supporting Information is available free of charge at https://pubs.acs.org/doi/10.1021/acsaem.3c02789.

Experimental methods used for the electrochemical measurements, HPLC standards, description of computational details, and experimental results of galvanostatic measurements (PDF)

AUTHOR INFORMATION

Corresponding Authors

Jai White − *Department of Chemical Engineering, KTH Royal Institute of Technology, Stockholm SE-100 44, Sweden;* orcid.org/0000-0002-9181-9825; Email: jaiw@kth.se

Egon Campos dos Santos − *FYSIKUM, AlbaNova University Center, Stockholm University, Stockholm SE-106 91, Sweden;* Present Address: Departamento de Física dos Materials e Mecânica, Instituto de Física, Universidade de São Paulo, São Paulo 05508-090, São Paulo, Brazil; orcid.org/0000-0002-8871-3368; Email: egoncs@gmail.com

Authors

Irina Terekhina − *Department of Materials and Environmental Chemistry, Stockholm University, Stockholm SE-10691, Sweden;* orcid.org/0000-0002-4759-5895

Daniel Martín-Yerga − *Department of Chemistry, Nanoscience Center, University of Jyväskylä, Jyväskylä FI-40014, Finland;* orcid.org/0000-0002-9385-7577

Lars G. M. Pettersson − *FYSIKUM, AlbaNova University Center, Stockholm University, Stockholm SE-106 91, Sweden*

Mats Johnsson − *Department of Materials and Environmental Chemistry, Stockholm University, Stockholm SE-10691, Sweden;* orcid.org/0000-0003-4319-1540

Ann Cornell − *Department of Chemical Engineering, KTH Royal Institute of Technology, Stockholm SE-100 44, Sweden;* orcid.org/0000-0001-5816-2924

Complete contact information is available at: https://pubs.acs.org/10.1021/acsaem.3c02789

Author Contributions

J.W., I.T., and E.C.d.S. contributed equally. The manuscript was written through contributions from all authors. All authors have given approval to the final version of the manuscript.

Notes

The authors declare no competing financial interest.

■ ACKNOWLEDGMENTS

The authors would like to acknowledge the Swedish Foundation for Strategic Research for funding this work through grant no. EM16-0010. The computations were enabled by resources provided by the National Academic Infrastructure for Supercomputing in Sweden (NAISS) and the Swedish National Infrastructure for Computing (SNIC) at the PDC and NSC centers partially funded by the Swedish Research Council through grant agreement nos. 2022-06725 and 2018-05973. D.M.-Y. thanks the Research Council of Finland for financial support (ref. 355569). The authors acknowledge that portions of this manuscript included the Ph.D. thesis written by J.W., entitled From Facets to Flow: The Electrooxidation of Glycerol on Pd-based catalysts (2023), for which J.W. holds the copyright (ISBN: 978-91-8040-752-6).

■ ABBREVIATIONS

CV, cyclic voltammetry; DFT, density functional theory; DHA, dihydroxyacetone; ECSA, electrochemical surface area; FA, formic acid/formate; GA, glycolic acid/glycolate; GD, glyceraldehyde; GEOR, glycerol electrooxidation reaction; GLA, glyceric acid/glycerate; Gly, glycerol; GOPs, glycerol oxidation products; HPA, hydroxypyruvic acid; ICPCs, *iR*-corrected polarization curves; LA, lactic acid; MLA, mesoxalic acid; NPs, nanoparticles; OA, oxalic acid/oxalate; PDS, potential determining step; PXRD, powder X-ray diffraction; RHE, reversible hydrogen electrode; TEM, transmission electron microscopy; TTA, tartronic acid/tartronate

■ REFERENCES

(1) Mahlia, T. M. I.; Syazmi, Z. A. H. S.; Mofijur, M.; Abas, A. P.; Bilad, M. R.; Ong, H. C.; Silitonga, A. S. Patent Landscape Review on Biodiesel Production: Technology Updates. *Renewable Sustainable Energy Rev.* **2020**, *118*, 109526.

(2) Likhanov, V. A.; Lopatin, O. P. Research of High-Speed Diesel Engines of Small Dimension on Biofuel. *J. Phys.: Conf. Ser.* **2019**, *1399* (5), 055016.

(3) *Biodiesel: From Production to Combustion*; Tabatabaei, M., Aghbashlo, M., Eds.; Biofuel and Biorefinery Technologies; Springer International Publishing: Cham, 2019; Vol. *8*..

(4) Ciriminna, R.; Pina, C. D.; Rossi, M.; Pagliaro, M. Understanding the Glycerol Market. *Eur. J. Lipid Sci. Technol.* **2014**, *116* (10), 1432−1439.

(5) Coutanceau, C.; Baranton, S.; Kouamé, R. S. B. Selective Electrooxidation of Glycerol Into Value-Added Chemicals: A Short Overview. *Front. Chem.* **2019**, *7*, 100.

(6) Simões, M.; Baranton, S.; Coutanceau, C. Electrochemical Valorisation of Glycerol. *ChemSusChem* **2012**, *5* (11), 2106−2124.

(7) Houache, M. S. E.; Hughes, K.; Baranova, E. A. Study on Catalyst Selection for Electrochemical Valorization of Glycerol. *Sustainable Energy Fuels* **2019**, *3* (8), 1892−1915.

(8) Holade, Y.; Tuleushova, N.; Tingry, S.; Servat, K.; Napporn, T. W.; Guesmi, H.; Cornu, D.; Kokoh, K. B. Recent Advances in the Electrooxidation of Biomass-Based Organic Molecules for Energy, Chemicals and Hydrogen Production. *Catal. Sci. Technol.* **2020**, *10* (10), 3071−3112.

(9) Wu, J.; Yang, X.; Gong, M. Recent Advances in Glycerol Valorization via Electrooxidation: Catalyst, Mechanism and Device. *Chin. J. Catal.* **2022**, *43* (12), 2966−2986.

(10) Ge, R.; Li, J.; Duan, H. Recent Advances in Non-Noble Electrocatalysts for Oxidative Valorization of Biomass Derivatives. *Sci. China Mater.* **2022**, *65* (12), 3273−3301.

(11) Simões, M.; Baranton, S.; Coutanceau, C. Electro-Oxidation of Glycerol at Pd Based Nano-Catalysts for an Application in Alkaline Fuel Cells for Chemicals and Energy Cogeneration. *Appl. Catal., B* **2010**, *93* (3−4), 354−362.

(12) Chen, X.; Granda-Marulanda, L. P.; McCrum, I. T.; Koper, M. T. M. How Palladium Inhibits CO Poisoning during Electrocatalytic Formic Acid Oxidation and Carbon Dioxide Reduction. *Nat. Commun.* **2022**, *13* (1), 38.

(13) Oliveira, V. L.; Morais, C.; Servat, K.; Napporn, T. W.; Tremiliosi-Filho, G.; Kokoh, K. B. Glycerol Oxidation on Nickel Based Nanocatalysts in Alkaline Medium - Identification of the Reaction Products. *J. Electroanal. Chem.* **2013**, *703*, 56−62.

(14) Holade, Y.; Morais, C.; Arrii-Clacens, S.; Servat, K.; Napporn, T. W.; Kokoh, K. B. New Preparation of PdNi/C and PdAg/C Nanocatalysts for Glycerol Electrooxidation in Alkaline Medium. *Electrocatalysis* **2013**, *4* (3), 167−178.

(15) Holade, Y.; Morais, C.; Servat, K.; Napporn, T. W.; Kokoh, K. B. Toward the Electrochemical Valorization of Glycerol: Fourier Transform Infrared Spectroscopic and Chromatographic Studies. *ACS Catal.* **2013**, *3* (10), 2403−2411.

(16) White, J.; Anil, A.; Martín-Yerga, D.; Salazar-Alvarez, G.; Henriksson, G.; Cornell, A. Electrodeposited PdNi on a Ni Rotating Disk Electrode Highly Active for Glycerol Electrooxidation in Alkaline Conditions. *Electrochim. Acta* **2022**, *403*, 139714.

(17) Koper, M. T. M. Structure Sensitivity and Nanoscale Effects in Electrocatalysis. *Nanoscale* **2011**, *3* (5), 2054−2073.

(18) Li, R.; Wei, Z.; Huang, T.; Yu, A. Ultrasonic-Assisted Synthesis of Pd-Ni Alloy Catalysts Supported on Multi-Walled Carbon Nanotubes for Formic Acid Electrooxidation. *Electrochim. Acta* **2011**, *56* (19), 6860−6865.

(19) Du, C.; Chen, M.; Wang, W.; Yin, G. Nanoporous PdNi Alloy Nanowires As Highly Active Catalysts for the Electro-Oxidation of Formic Acid. *ACS Appl. Mater. Interfaces* **2011**, *3* (2), 105−109.

(20) López-Coronel, A.; Torres-Pacheco, L. J.; Bañuelos, J. A.; Álvarez-López, A.; Guerra-Balcázar, M.; Álvarez-Contreras, L.; Arjona, N. Highly Active PdNi Bimetallic Nanocubes Electrocatalysts for the Ethylene Glycol Electro-Oxidation in Alkaline Medium. *Appl. Surf. Sci.* **2020**, *530*, 147210.

(21) Guo, M.; Wang, H.; Cui, L.; Zhang, J.; Xiang, Y.; Lu, S. Nickel Promoted Palladium Nanoparticles for Electrocatalysis of Carbohydrazide Oxidation Reaction. *Small* **2019**, *15* (28), 1900929.

(22) Shen, S. Y.; Zhao, T. S.; Xu, J. B.; Li, Y. S. Synthesis of PdNi Catalysts for the Oxidation of Ethanol in Alkaline Direct Ethanol Fuel Cells. *J. Power Sources* **2010**, *195* (4), 1001−1006.

(23) Miao, B.; Wu, Z.-P.; Zhang, M.; Chen, Y.; Wang, L. Role of Ni in Bimetallic PdNi Catalysts for Ethanol Oxidation Reaction. *J. Phys. Chem. C* **2018**, *122* (39), 22448−22459.

(24) Yang, H.; Wang, H.; Li, H.; Ji, S.; Davids, M. W.; Wang, R. Effect of Stabilizers on the Synthesis of Palladium-Nickel Nanoparticles Supported on Carbon for Ethanol Oxidation in Alkaline Medium. *J. Power Sources* **2014**, *260*, 12−18.

(25) Dutta, A.; Datta, J. Energy Efficient Role of Ni/NiO in PdNi Nano Catalyst Used in Alkaline DEFC. *J. Mater. Chem. A* **2014**, *2* (9), 3237−3250.

(26) Zhao, Y.; Yang, X.; Tian, J.; Wang, F.; Zhan, L. Methanol Electro-Oxidation on Ni@Pd Core-Shell Nanoparticles Supported on Multi-Walled Carbon Nanotubes in Alkaline Media. *Int. J. Hydrogen Energy* **2010**, *35* (8), 3249−3257.

(27) Araujo, R. B.; Martín-Yerga, D.; Santos, E. C.; Cornell, A.; Pettersson, L. G. M. Elucidating the Role of Ni to Enhance the Methanol Oxidation Reaction on Pd Electrocatalysts. *Electrochim. Acta* **2020**, *360*, 136954.

(28) Liu, Z.; Zhang, X.; Hong, L. Physical and Electrochemical Characterizations of Nanostructured Pd/C and PdNi/C Catalysts for Methanol Oxidation. *Electrochem. Commun.* **2009**, *11* (4), 925−928.

(29) Martín-Yerga, D.; Yu, X.; Terekhina, I.; Henriksson, G.; Cornell, A. In Situ Catalyst Reactivation for Enhancing Alcohol Electro-Oxidation and Coupled Hydrogen Generation. *Chem. Commun.* **2020**, *56* (28), 4011−4014.

https://doi.org/10.1021/acsaem.3c02789
ACS Appl. Energy Mater. 2024, 7, 1802−1813

(30) Martín-Yerga, D.; White, J.; Henriksson, G.; Cornell, A. Structure-Reactivity Effects of Biomass-Based Hydroxyacids for Sustainable Electrochemical Hydrogen Production. *ChemSusChem* **2021**, *14* (8), 1902−1912.
(31) Ipadeola, A. K.; Lisa Mathebula, N. Z.; Pagliaro, M. V.; Miller, H. A.; Vizza, F.; Davies, V.; Jia, Q.; Marken, F.; Ozoemena, K. I. Unmasking the Latent Passivating Roles of Ni(OH)2 on the Performance of Pd-Ni Electrocatalysts for Alkaline Ethanol Fuel Cells. *ACS Appl. Energy Mater.* **2020**, *3* (9), 8786−8802.
(32) del Rosario, J. A. D.; Ocon, J. D.; Jeon, H.; Yi, Y.; Lee, J. K.; Lee, J. Enhancing Role of Nickel in the Nickel-Palladium Bilayer for Electrocatalytic Oxidation of Ethanol in Alkaline Media. *J. Phys. Chem. C* **2014**, *118* (39), 22473−22478.
(33) White, J.; Peters, L.; Martín-Yerga, D.; Terekhina, I.; Anil, A.; Lundberg, H.; Johnsson, M.; Salazar-Alvarez, G.; Henriksson, G.; Cornell, A. Glycerol Electrooxidation at Industrially Relevant Current Densities Using Electrodeposited PdNi/Nifoam Catalysts in Aerated Alkaline Media. *J. Electrochem. Soc.* **2023**, *170* (8), 086504.
(34) Hiltrop, D.; Cychy, S.; Elumeeva, K.; Schuhmann, W.; Muhler, M. Spectroelectrochemical Studies on the Effect of Cations in the Alkaline Glycerol Oxidation Reaction over Carbon Nanotube-Supported Pd Nanoparticles. *Beilstein J. Org. Chem.* **2018**, *14* (1), 1428−1435.
(35) Rahim, S. A. N. M.; Lee, C. S.; Abnisa, F.; Aroua, M. K.; Daud, W. A. W.; Cognet, P.; Pérès, Y. A Review of Recent Developments on Kinetics Parameters for Glycerol Electrochemical Conversion - A by-Product of Biodiesel. *Sci. Total Environ.* **2020**, *705*, 135137.
(36) Rodrigues, T. S.; Zhao, M.; Yang, T.-H.; Gilroy, K. D.; da Silva, A. G. M.; Camargo, P. H. C.; Xia, Y. Synthesis of Colloidal Metal Nanocrystals: A Comprehensive Review on the Reductants. *Chem.—Eur. J.* **2018**, *24* (64), 16944−16963.
(37) Poerwoprajitno, A. R.; Gloag, L.; Cheong, S.; Gooding, J. J.; Tilley, R. D. Synthesis of Low- and High-Index Faceted Metal (Pt, Pd, Ru, Ir, Rh) Nanoparticles for Improved Activity and Stability in Electrocatalysis. *Nanoscale* **2019**, *11* (41), 18995−19011.
(38) Gilroy, K. D.; Ruditskiy, A.; Peng, H.-C.; Qin, D.; Xia, Y. Bimetallic Nanocrystals: Syntheses, Properties, and Applications. *Chem. Rev.* **2016**, *116* (18), 10414−10472.
(39) Göksu, H.; Ho, S. F.; Metin, O.; Korkmaz, K.; Mendoza Garcia, A.; Gültekin, M. S.; Sun, S. Tandem Dehydrogenation of Ammonia Borane and Hydrogenation of Nitro/Nitrile Compounds Catalyzed by Graphene-Supported NiPd Alloy Nanoparticles. *ACS Catal.* **2014**, *4* (6), 1777−1782.
(40) Hummelgård, C.; Karlsson, R. K. B.; Bäckström, J.; Rahman, S. M. H.; Cornell, A.; Eriksson, S.; Olin, H. Physical and Electrochemical Properties of Cobalt Doped (Ti,Ru)O2 Electrode Coatings. *Mater. Sci. Eng. B* **2013**, *178* (20), 1515−1522.
(41) Bolzán, A. Phenomenological Aspects Related to the Electrochemical Behaviour of Smooth Palladium Electrodes in Alkaline Solutions. *J. Electroanal. Chem.* **1995**, *380* (1−2), 127−138.
(42) Breiter, M. W. Dissolution and Adsorption of Hydrogen at Smooth Pd Wires of the Alpha Phase in Sulfuric Acid Solution. *J. Electroanal. Chem.* **1977**, *81* (2), 275−284.
(43) Chierchie, T.; Mayer, C.; Lorenz, W. J. Structural Changes of Surface Oxide Layers on Palladium. *J. Electroanal. Chem.* **1982**, *135*, 211−220.
(44) Hjorth Larsen, A.; Jørgen Mortensen, J.; Blomqvist, J.; Castelli, I. E.; Christensen, R.; Dułak, M.; Friis, J.; Groves, M. N.; Hammer, B.; Hargus, C.; Hermes, E. D.; Jennings, P. C.; Bjerre Jensen, P.; Kermode, J.; Kitchin, J. R.; Leonhard Kolsbjerg, E.; Kubal, J.; Kaasbjerg, K.; Lysgaard, S.; Bergmann Maronsson, J.; Maxson, T.; Olsen, T.; Pastewka, L.; Peterson, A.; Rostgaard, C.; Schiøtz, J.; Schütt, O.; Strange, M.; Thygesen, K. S.; Vegge, T.; Vilhelmsen, L.; Walter, M.; Zeng, Z.; Jacobsen, K. W. The Atomic Simulation Environment-a Python Library for Working with Atoms. *J. Phys.: Condens. Matter* **2017**, *29* (27), 273002.
(45) Kresse, G.; Furthmüller, J. Efficient Iterative Schemes for Ab Initio Total-Energy Calculations Using a Plane-Wave Basis Set. *Phys. Rev. B* **1996**, *54* (16), 11169−11186.
(46) Wellendorff, J.; Lundgaard, K. T.; Møgelhøj, A.; Petzold, V.; Landis, D. D.; Nørskov, J. K.; Bligaard, T.; Jacobsen, K. W. Density Functionals for Surface Science: Exchange-Correlation Model Development with Bayesian Error Estimation. *Phys. Rev. B* **2012**, *85* (23), 235149.
(47) Anil, A.; White, J.; Campos dos Santos, E.; Terekhina, I.; Johnsson, M.; Pettersson, L. G. M.; Cornell, A.; Salazar-Alvarez, G. Effect of Pore Mesostructure on the Electrooxidation of Glycerol on Pt Mesoporous Catalysts. *J. Mater. Chem. A* **2023**, *11* (31), 16570−16577.
(48) dos Santos, E. C.; Araujo, R. B.; Valter, M.; Salazar-Alvarez, G.; Johnsson, M.; Bajdich, M.; Abild-Pedersen, F.; Pettersson, L. G. M. Efficient Screening of Bi-Metallic Electrocatalysts for Glycerol Valorization. *Electrochim. Acta* **2021**, *398*, 139283.
(49) T. C., Allison. NIST-JANAF Thermochemical Tables - SRD 13, **2013**. .
(50) Mathew, K.; Sundararaman, R.; Letchworth-Weaver, K.; Arias, T. A.; Hennig, R. G. Implicit Solvation Model for Density-Functional Study of Nanocrystal Surfaces and Reaction Pathways. *J. Chem. Phys.* **2014**, *140* (8), 084106.
(51) Nørskov, J. K.; Rossmeisl, J.; Logadottir, A.; Lindqvist, L.; Kitchin, J. R.; Bligaard, T.; Jónsson, H. Origin of the Overpotential for Oxygen Reduction at a Fuel-Cell Cathode. *J. Phys. Chem. B* **2004**, *108* (46), 17886−17892.
(52) Sen, B.; Kuzu, S.; Demir, E.; Yıldırır, E.; Sen, F. Highly Efficient Catalytic Dehydrogenation of Dimethyl Ammonia Borane via Monodisperse Palladium-Nickel Alloy Nanoparticles Assembled on PEDOT. *Int. J. Hydrogen Energy* **2017**, *42* (36), 23307−23314.
(53) Matin, M. A.; Jang, J.-H.; Kwon, Y.-U. PdM Nanoparticles (M = Ni, Co, Fe, Mn) with High Activity and Stability in Formic Acid Oxidation Synthesized by Sonochemical Reactions. *J. Power Sources* **2014**, *262*, 356−363.
(54) Khan, M. S.; Khattak, R.; Khan, A.; Chen, Q.; Nisar, J.; Iqbal, Z.; Rashid, A.; Kamran, A. W.; Zekker, I.; Zahoor, M.; Alzahrani, K. J.; Batiha, G. E.-S. Synthesis and Characterizations of PdNi Carbon Supported Nanomaterials: Studies of Electrocatalytic Activity for Oxygen Reduction in Alkaline Medium. *Molecules* **2021**, *26* (11), 3440.
(55) Wang, L.; Dong, K. J.; Wang, C. C.; Zou, R. P.; Zhou, Z. Y.; Yu, A. B. Computer Simulation of the Packing of Nanoparticles. *Powder Technol.* **2022**, *401*, 117317.
(56) Eldridge, M. D.; Madden, P. A.; Frenkel, D. Entropy-Driven Formation of a Superlattice in a Hard-Sphere Binary Mixture. *Nature* **1993**, *365* (6441), 35−37.
(57) Wang, Z.; Schliehe, C.; Bian, K.; Dale, D.; Bassett, W. A.; Hanrath, T.; Klinke, C.; Weller, H. Correlating Superlattice Polymorphs to Internanoparticle Distance, Packing Density, and Surface Lattice in Assemblies of PbS Nanoparticles. *Nano Lett.* **2013**, *13* (3), 1303−1311.
(58) Bouju, X.; Duguet, É.; Gauffre, F.; Henry, C. R.; Kahn, M. L.; Mélinon, P.; Ravaine, S. Nonisotropic Self-Assembly of Nanoparticles: From Compact Packing to Functional Aggregates. *Adv. Mater.* **2018**, *30* (27), 1706558.
(59) Wang, L.; Lavacchi, A.; Bellini, M.; D'Acapito, F.; Benedetto, F. D.; Innocenti, M.; Miller, H. A.; Montegrossi, G.; Zafferoni, C.; Vizza, F. Deactivation of Palladium Electrocatalysts for Alcohols Oxidation in Basic Electrolytes. *Electrochim. Acta* **2015**, *177*, 100−106.
(60) Daily Metal Price: Palladium Price (USD/Gram) Chart for the Last Week. https://www.dailymetalprice.com/metalpricecharts.php?c=pd&u=oz&d=240 (accessed 10 16, 2023).
(61) Daily Metal Price: Nickel Price (USD/Gram) Chart for the Last Week. https://www.dailymetalprice.com/metalpricecharts.php?c=ni&u=lb&d=0 (accessed 10 16, 2023).
(62) Oliveira, V. L.; Morais, C.; Servat, K.; Napporn, T. W.; Tremiliosi-Filho, G.; Kokoh, K. B. Glycerol Oxidation on Nickel Based Nanocatalysts in Alkaline Medium - Identification of the Reaction Products. *J. Electroanal. Chem.* **2013**, *703*, 56.
(63) Goetz, M. K.; Bender, M. T.; Choi, K.-S. Predictive Control of Selective Secondary Alcohol Oxidation of Glycerol on NiOOH. *Nat. Commun.* **2022**, *13* (1), 5848.

(64) Zhang, N.; Wang, J.; Zhang, W.; Zhao, Y.; Dong, Z.; Wu, Z.; Xu, G.-R.; Wang, L. Self-Supported PdNi Dendrite on Ni Foam for Improving Monohydric Alcohol and Polyhydric Alcohols Electrooxidation. *Fuel* **2022**, *326*, 125083.
(65) Luo, H.; Yukuhiro, V. Y.; Fernández, P. S.; Feng, J.; Thompson, P.; Rao, R. R.; Cai, R.; Favero, S.; Haigh, S. J.; Durrant, J. R.; Stephens, I. E. L.; Titirici, M.-M. Role of Ni in PtNi Bimetallic Electrocatalysts for Hydrogen and Value-Added Chemicals Coproduction via Glycerol Electrooxidation. *ACS Catal.* **2022**, *12* (23), 14492−14506.
(66) Mphahlele, N. E.; Ipadeola, A. K.; Haruna, A. B.; Mwonga, P. V.; Modibedi, R. M.; Palaniyandy, N.; Billing, C.; Ozoemena, K. I. Microwave-induced Defective PdFe/C Nano-electrocatalyst for Highly Efficient Alkaline Glycerol Oxidation Reactions. *Electrochim. Acta* **2022**, *409*, 139977.
(67) Houache, M. S. E.; Shubair, A.; Sandoval, M. G.; Safari, R.; Botton, G. A.; Jasen, P. V.; González, E. A.; Baranova, E. A. Influence of Pd and Au on Electrochemical Valorization of Glycerol over Ni-Rich Surfaces. *J. Catal.* **2021**, *396*, 1−13.
(68) Wang, H.; Thia, L.; Li, N.; Ge, X.; Liu, Z.; Wang, X. Pd Nanoparticles on Carbon Nitride-Graphene for the Selective Electro-Oxidation of Glycerol in Alkaline Solution. *ACS Catal.* **2015**, *5* (6), 3174−3180.
(69) Melle, G.; de Souza, M. B. C.; Santiago, P. V. B.; Corradini, P. G.; Mascaro, L. H.; Fernández, P. S.; Sitta, E. Glycerol Electro-Oxidation at Pt in Alkaline Media: Influence of Mass Transport and Cations. *Electrochim. Acta* **2021**, *398*, 139318.
(70) Zhou, Y.; Shen, Y.; Piao, J. Sustainable Conversion of Glycerol into Value-Added Chemicals by Selective Electro-Oxidation on Pt-Based Catalysts. *ChemElectroChem* **2018**, *5* (13), 1636−1643.
(71) Valter, M.; dos Santos, E. C.; Pettersson, L. G. M.; Hellman, A. Partial Electrooxidation of Glycerol on Close-Packed Transition Metal Surfaces: Insights from First-Principles Calculations. *J. Phys. Chem. C* **2020**, *124* (33), 17907−17915.
(72) Valter, M.; Santos, E. C.; Pettersson, L. G. M.; Hellman, A. Selectivity of the First Two Glycerol Dehydrogenation Steps Determined Using Scaling Relationships. *ACS Catal.* **2021**, *11* (6), 3487−3497.
(73) Yu, X.; dos Santos, E. C.; White, J.; Salazar-Alvarez, G.; Pettersson, L. G. M.; Cornell, A.; Johnsson, M. Electrocatalytic Glycerol Oxidation with Concurrent Hydrogen Evolution Utilizing an Efficient MoOx/Pt Catalyst. *Small* **2021**, *17* (44), 2104288.
(74) Yaylayan, V.; Harty-Majors, S.; Ismail, A. Investigation of Dl-Glyceraldehyde-Dihydroxyacetone Interconversion by FTIR Spectroscopy. *Carbohydr. Res.* **1999**, *318* (1−4), 20−25.
(75) Rasrendra, C. B.; Fachri, B. A.; Makertihartha, I. G. B. N.; Adisasmito, S.; Heeres, H. J. Catalytic Conversion of Dihydroxyacetone to Lactic Acid Using Metal Salts in Water. *ChemSusChem* **2011**, *4* (6), 768−777.
(76) Denis, W. On the Behaviour of Various Aldehydes, Ketones and Alcohols towards Oxidizing Agents. *Am. Chem. J.* **1907**, *38*, 561−594.
(77) Fedoroňko, M.; Königstein, J. Kinetics of Mutual Isomerization of Trioses and Their Dehydration to Methylglyoxal. *Collect. Czech. Chem. Commun.* **1969**, *34*, 3881−3894.

https://doi.org/10.1021/acsaem.3c02789
ACS Appl. Energy Mater. 2024, 7, 1802−1813